Geosci. Model Dev. Discuss., 8, 9373–9413, 2015
www.geosci-model-dev-discuss.net/8/9373/2015/
doi:10.5194/gmdd-8-9373-2015

Geoscientific Model Development Discussions
Open Access

Air Quality Modeling with WRF-Chem v3.5 in East and South Asia: sensitivity to emissions and evaluation of simulated air quality

M. Zhong[1], E. Saikawa[1,2], Y. Liu[2], V. Naik[3,4], L. W. Horowitz[3], M. Takigawa[5], Y. Zhao[6], N.-H. Lin[7], and E. A. Stone[8]

[1]Department of Environmental Sciences, Emory University, Atlanta, GA, USA
[2]Department of Environmental Health, Rollins School of Public Health, Emory University, Atlanta, GA, USA
[3]NOAA Geophysical Fluid Dynamics Laboratory, Princeton, NJ, USA
[4]University Corporation for Atmospheric Research, Boulder, CO, USA
[5]Japan Agency for Marine-Earth Science and Technology, Yokohama, Japan
[6]Nanjing University, Nanjing, China
[7]Department of Atmospheric Sciences, National Central University, Chuang-Li, Taiwan
[8]Department of Chemistry, University of Iowa, Iowa City, IA, USA

Received: 1 September 2015 – Accepted: 5 September 2015 – Published: 29 October 2015

Correspondence to: M. Zhong (min.zhong@emory.edu)
and E. Saikawa (eri.saikawa@emory.edu)

Published by Copernicus Publications on behalf of the European Geosciences Union.

Abstract

We conducted simulations using the Weather Research and Forecasting model coupled with Chemistry (WRF-Chem) version 3.5 to study air quality in East and South Asia at a spatial resolution of 20 km × 20 km. We find large discrepancies between two existing emissions inventories: the Regional Emission Inventory in Asia version 2 (REAS) and the Emissions Database for Global Atmospheric Research version 4.2 (EDGAR) at the provincial level in China, with maximum differences up to 500 % for CO emissions, 190 % for NO, and 160 % for primary PM_{10}. Such differences in the magnitude and the spatial distribution of emissions for various species lead to 40–70 % difference in surface PM_{10} concentrations, 16–20 % in surface O_3 mixing ratios, and over 100 % in SO_2 and NO_2 mixing ratios in the polluted areas of China. Our sensitivity run shows WRF-Chem is sensitive to emissions, with the REAS-based simulation reproducing observed concentrations and mixing ratios better than the EDGAR-based simulation for July 2007. We conduct further model simulations using REAS emissions for January, April, July, and October in 2007 and evaluate simulations with available ground-level observations. The model results show clear regional variations in the seasonal cycle of surface PM_{10} and O_3 over East and South Asia. The model meets the air quality model performance criteria for both PM_{10} (mean fractional bias, MFB $\leqslant \pm 60\,\%$) and O_3 (MFB $\leqslant \pm 15\,\%$) in most of the observation sites, although the model underestimates PM_{10} over Northeast China in January. The model predicts the observed SO_2 well at sites in Japan, while it tends to overestimate SO_2 in China in July and October. The model underestimates most observed NO_2 in all four months. These findings suggest that future model development and evaluation of emission inventories and models are needed for particulate matter and gaseous pollutants in East and South Asia.

1 Introduction

Many East and South Asian countries have faced deteriorating air quality since the late 1990s and early 2000s due to rapid economic development and population growth. According to the latest World Health Organization (WHO) ambient air pollution database (WHO, 2014), air quality in China and India were ranked 14th and 9th respectively, out of the 91 most polluted countries. Since these countries have the largest population in the world, exposure to air pollutants poses health risks to billions of residents. For example, Chen et al. (2013) reported that outdoor air pollution in China alone caused approximately half a million premature deaths every year. A similar number of premature deaths was estimated in India in 2010 (HEI, 2013). Air pollution not only impacts human health, but also has important potential consequences for natural ecosystems, crop yields, visibility, and radiative forcing (Seinfeld and Pandis, 2012). In order to mitigate these negative consequences, it is essential to have a better understanding of air pollutant emission sources and magnitudes, as well as atmospheric transport and chemical composition over the region.

Several modeling studies have applied the Weather Research and Forecasting model coupled with Chemistry (WRF-Chem) (Grell et al., 2005) to study air quality in Asia. Saikawa et al. (2011) analyzed the impact of China's vehicle emissions on air quality both within China and across East Asia. They found that stricter regulation of the road transport sector in China would reduce surface concentrations of fine particulate matter with an aerodynamic diameter of 2.5 µm or less ($PM_{2.5}$) and tropospheric ozone (O_3) mixing ratios in the region. Kumar et al. (2012) examined ground level measurements and satellite observations in South Asia and reported that WRF-Chem could simulated O_3 and CO well but large discrepancies were found for NO_2 due to uncertainties in biomass burning emissions and anthropogenic NOx estimates. Wang et al. (2010) conducted sensitivity analyses of O_3, NO_x, and sulfur dioxide (SO_2) mixing ratios to temporal and vertical emissions; their results showed that air quality in East Asia was impacted by the diurnal and vertical distribution of anthropogenic emissions.

GMDD
8, 9373–9413, 2015

Air Quality Modeling with WRF-Chem v3.5 in East and South Asia

M. Zhong et al.

Studies that have conducted WRF-Chem modeling for $PM_{2.5}$ and PM_{10} have found that these surface concentrations were usually underestimated. For example, Saikawa et al. (2011) reported that modeled four month average $PM_{2.5}$ concentrations at Oki and Rishiri in Japan had a mean normalized bias (MNB) of −34 % compared to observations. Gao et al. (2014) compared simulated and measured PM_{10} concentrations at six sites in Japan and found that the model underestimated the annual average PM_{10} at all sites except one.

One of the possible reasons that models underestimate particulate matter (PM) concentrations is the uncertainty in emissions. We find that the difference in anthropogenic emissions estimated by different emission inventories can differ by up to 160 % for primary PM_{10} at the provincial level in China. Since the simulated concentrations of pollutants are linked to emissions, such high emission discrepancies at the provincial level are expected to affect air quality simulations. A few studies have investigated the influence of anthropogenic emission inventories on air quality. Ma and van Aardenne (2004) compared simulated surface O_3 mixing ratios over China using three different emission inventories as model inputs, and found that surface O_3 differed as much as 30–50 % among different model simulations. They also demonstrated that the differences in NO_x and non-methane volatile organic compounds (NMVOCs) among different inventories were dominant factors for the discrepancies in simulated O_3 mixing ratios. Amnuaylojaroen et al. (2014), on the other hand, studied the effect of different anthropogenic emission inventories on air quality over Southeast Asia and they found only a small difference in simulated O_3 (about 4.5 %) and CO (about 8 %) mixing ratios. However, these studies did not investigate the impact of emission inventories on other pollutant species such as PM.

The first objective of this paper is to study the sensitivity of regional air quality to emissions. We select two commonly used anthropogenic emission inventories for comparison: the Regional Emission Inventory in ASia version 2 (REAS) (Kurokawa et al., 2013) and the Emissions Database for Global Atmospheric Research version 4.2 (EDGAR) (JRC and PBL, 2010). By comparing the 2-week model simulations using these two emission inventories and the observations for July 2007, we select the REAS inventory to perform air quality simulations over East and South Asia in different seasons. The second objective is to evaluate the simulated PM_{10} concentrations, as well as O_3, SO_2, and NO_x mixing ratios from four one-month WRF-Chem runs against ground-level observations to build confidence in its ability to simulate future air quality over this region. So far, many of the WRF-Chem studies that focused over China conducted limited model evaluation due to the scarcity of observations in the region. This study compares the model simulations to observations from more than 70 sites in China to evaluate the model. There are some studies that have compared simulation results using a different chemical transport model (i.e., the Community Multi-scale Air Quality Model), but as far as we are aware, few studies used as extensive a network of observations for WRF-Chem validation in this region.

This paper is organized as follows. Section 2 explains the regional air quality model (WRF-Chem) configuration, emissions used for the model, observations used for validation, and data analysis methods. Section 3 analyzes the differences in emission inventories and the sensitivity of simulated pollutant concentrations to the inventory used. In Sect. 4, model performance is evaluated by comparing observations with model simulations. Section 5 presents a summary of results and suggestions for future research.

2 Model and observations description

2.1 Model description

We use the fully coupled "online" regional chemical transport model WRF-Chem version 3.5 (Grell et al., 2005) in this study. The Regional Acid Deposition Model version 2 (RADM2) atmospheric chemical mechanism (Stockwell et al., 1990) is used for gas-phase chemistry. Aerosol chemistry is represented by the Model Aerosol Dynamics for Europe with the Secondary Organic Aerosol Model (MADE/SORGAM) (Schell et al., 2001; Ackermann et al., 1998) with some aqueous reactions. This aerosol mechanism is widely used in regional atmospheric chemistry models (Saikawa et al., 2011; Gao et al., 2014; Tuccella et al., 2012; Kumar et al., 2012). It predicts the mass of seven aerosol species (sulfate, ammonium, nitrate, sea salt, BC, OC, and secondary organic aerosols), using three log-normal aerosol modes (Aitken, accumulation, and coarse). Aerosol dry deposition is simulated following the approach of Binkowski and Shankar (1995) and the wet removal follows Easter et al. (2004) and Chapman et al. (2009). Photolysis rates are obtained from the Fast-J photolysis scheme (Wild et al., 2000). We use the Lin et al. (1983) microphysics scheme and the Grell-3d ensemble cumulus parameterization (Grell and Dévényi, 2002).

The model domain, shown in Fig. 1, covers most of the East and South Asia region with 398 × 298 grid cells, using a 20 km spacing and a Lambert conformal map projection centered on China at 32° N, 100° E. There are 31 vertical levels from the surface to 50 mb. The initial and lateral boundary conditions are taken from a time-slice simulation of the GFDL coupled chemistry-climate model AM3 (Donner et al., 2011; Naik et al., 2013) for year 2010 following the configuration described by Naik et al. (2013). This AM3 simulation was driven by climatological mean sea-surface temperature and sea ice distributions for the 2006–2015 time period derived from the transient GFDL coupled model (GFDL-CM3) simulations following the Representative Concentration Pathway 8.5 (RCP8.5) (John et al., 2012). Concentrations of well-mixed greenhouse gases and ozone depleting substances, and emissions of short-lived pollutants (ozone precursors and aerosols) were set to year 2010 values in RCP8.5. The 2007 meteorological data are obtained from the National Center for Environmental Prediction (NCEP) Global Forecast System final gridded analysis datasets. We simulate air pollutant concentrations for the central month of each season (January, April, July, and October) in 2007, to assess seasonal variability in air quality. The model is spun-up for seven days before the beginning of each monthly simulation, sufficient to ventilate our regional domain.

GMDD
8, 9373–9413, 2015

2.2 Emissions

The anthropogenic emissions of gaseous pollutants (CO, NO_x, NH_3, SO_2, and NMVOCs) and particulate matter (BC, OC, $PM_{2.5}$, and PM_{10}) are taken from REAS (Kurokawa et al., 2013). REAS covers most of the model domain (see Fig. 1, regions in blue). For the areas of our domain that are not covered by the REAS emissions inventory, we use the RCP8.5 emission dataset for year 2010 (Riahi et al., 2011). RCP8.5 emission dataset has been used in many studies for air quality simulations (Gao et al., 2013; Colette et al., 2013; Fry et al., 2012). For biomass burning emissions, we use the year 2007 from the Global Fire Emissions Database version 3 (GFED) (Randerson et al., 2013). For biogenic emissions of CO, NO_x, and NMVOCs, as well as aircraft emissions of CO, NO_x, and SO_2, we use the Precursors of Ozone and their Effect on the Troposphere version 1 (POET) emissions inventory (Granier et al., 2005). Dust and sea salt emissions are calculated online using the dust transport model (Shaw et al., 2008) and sea salt (Gong, 2003) schemes, respectively.

To study the influence of anthropogenic emission inventories on air quality simulation, we conducted a sensitivity simulation using the EDGAR (European Commission Joint Research Centre, 2010) inventory, as described in Sect. 3. EDGAR does not provide BC, OC, and $PM_{2.5}$ emissions and thus this study only compares simulated O_3 and PM_{10}. NMVOCs in EDGAR are also not speciated, so we divided them into 17 chemical species, using weighting factors calculated from REAS. The total anthropogenic emissions of each air pollutant within the model domain as estimated in REAS and EDGAR for July 2007 are listed in Table 1.

2.3 Observations

The surface concentrations of PM_{10} in China are derived from the Air Pollution Index (API) from the website of the Ministry of Environmental Protection of the People's Republic of China (http://datacenter.mep.gov.cn/). When PM_{10} is reported as the primary pollutant with a maximum pollutant index, daily PM_{10} concentrations are calculated from the API, using the following equation:

$$C = [(I - I_{low})/(I_{high} - I_{low})] \times (C_{high} - C_{low}) + C_{low} \tag{1}$$

where C is the daily concentration of PM_{10}, I is the API reported, I_{low} and I_{high} are the lower and upper API breakpoints that I falls in, C_{low} and C_{high} are the PM_{10} concentrations corresponding to I_{low} and I_{high}. Values of I_{low}, I_{high}, C_{low} and C_{high} are described for different API levels, as shown in Table S1 in the Supplement. Qu et al. (2010) have shown that API-derived PM_{10} concentrations are generally comparable with those from filter sampling, although the latter tends to be approximately 10 % higher than API-derived PM_{10}. As mentioned earlier, the derived concentrations from API have been used for the evaluation of a different chemical transport model from previous studies (Wang et al., 2009; Liu et al., 2010).

The observed PM_{10} concentrations in Nepal are obtained from the Godavari station, located at the southern edge of the Kathmandu Valley (Ramanathan et al., 2007; Stone et al., 2010). The observed PM_{10}, O_3, and SO_2 in Japan and SO_2 and NO_2 in China are taken from the Acid Deposition Monitoring Network in East Asia (EANET). The surface mixing ratios of O_3 in Mt. Lulin are taken from the Lulin Atmospheric Background Station (LABS, 2862m above mean sea leave) in central Taiwan (Ou Yang et al., 2012). The description of each site is listed in Tables S2a–b; the locations of these sites are shown in Fig. 1.

2.4 Data analysis method

We assess the model performance using the correlation coefficient (r), the normalized mean bias (NMB), the mean fractional bias (MFB), the mean fractional error (MFE), and the normalized mean square error (NMSE) between the observed (Obs) and modeled (Model) concentrations. The performance evaluation is based on monthly and yearly statistics using the daily mean values at each site, each region, and all sites. For PM_{10}, we use the performance goals and criteria of Boylan and Russell (2006). Following their suggestion, we set goals and criteria for MFB to be less than or equal to ±30 and ±60 %, respectively. Goals and criteria for MFE are less than or equal to 50 % and 75 %, respectively. For O_3, we use the performance benchmark: MFB $\leqslant \pm 15$ % and MFE $\leqslant 35$ %, as recommended by Morris et al. (2005).

3 Sensitivity to emissions

To better understand the effect that anthropogenic emissions have on regional air quality simulations, we conduct two simulations in which REAS and EDGAR are used as separate inputs. In the following sections, we compare the major pollutant emissions estimated in REAS and EDGAR, followed by comparisons of resulting air quality simulations.

3.1 Emission comparisons

Table 1 summarizes the total emissions of major air pollutants over the model domain in July 2007 for air pollutant precursors. Both REAS and EGAR estimate similar total SO_2 emissions of 4.62 Tg month^{-1}. We, however, find large discrepancies between REAS and EDGAR estimated emissions for total NH_3 (53 %) and NO_x (27 %). For CO, NH_3, and NO_x, REAS estimates are higher than EDGAR, while for PM_{10} and NMVOCs, the opposite is the case. Figure 2 illustrates the difference in the spatial distribution and magnitude of emissions between REAS and EDGAR for PM_{10}, CO, SO_2, and NO_x in our model domain. Although the total emissions within the domain for many of the species are comparable between the two inventories, the national and regional differences are large. REAS estimates are uniformly higher than EDGAR in North, East, and South China for all four species and in most parts of India for NO_x and CO. For PM_{10} and CO, EDGAR estimates are higher in most areas of South and Southeast Asia, as well as in Japan and South Korea. Table S3 compares the differences in provincial emissions between REAS and EDGAR in China. For example, we find that REAS estimates 150 % higher PM_{10} and 548 % higher CO emissions than

GMDD
8, 9373–9413, 2015

EDGAR in Hebei province. The possible cause of such large national and regional discrepancies between REAS and EDGAR is differences in: (1) estimated activity level, (2) level of estimated technologies implemented, and (3) emission factors used in the emission calculations (Kurokawa et al., 2013; JRC and PBL, 2010). In this paper we focus on analyzing the impact of such discrepancies, rather than the cause of them.

3.2 Simulation comparisons

For the convenience of discussion, we name the simulation with REAS emissions as WRF-Chem-REAS and the simulation using EDGAR emissions as WRF-Chem-EDGAR. Figure 3 illustrates the differences in the 14-day mean PM_{10}, O_3, SO_2, and NO_2 simulated from 1 July to 14 July 2007. The difference is presented as the percentage difference in concentrations or mixing ratios relative to those simulated in WRF-Chem-EDGAR. The pattern of the difference for these species is similar to that of emissions difference. WRF-Chem-REAS simulates 40–70 % higher surface PM_{10} in most areas of the North China Plain (Beijing, Tianjin, Hebei, Henan, Shandong province). This difference, around 35 $\mu g\,m^{-3}$ or higher, is comparable to the PM_{10} levels in many sites in Japan (Table 3). The highest difference (70 %) occurs in Shandong province and the lowest difference (less than ±5 %) is found in western China (Table S3). WRF-Chem-EDGAR simulates higher PM_{10} than WRF-Chem-REAS around Cambodia, Vietnam, and Thailand. For surface O_3, a moderate difference of 16–20 % (approximately 12–16 ppbv) is found over the North China Plain, the Yangtze River Delta, Central China, and eastern Pakistan. WRF-Chem-REAS also results in higher SO_2 and NO_2 (more than 10 ppbv) in these areas than WRF-Chem-EDGAR. The large discrepancies, over 100 %, occur in Guizhou (220 %) and Yunnan (175 %) provinces for SO_2, and in Shanghai (258 %) and Shandong (118 %) provinces for NO_2.

Table 2 summarizes the statistical measures of model simulations using these two anthropogenic emissions inventories against observations. Both simulations reproduce the temporal variation of O_3, SO_2, and NO_2 well, with the value of r between 0.64 and 0.83. The temporal correlation of PM_{10} for WRF-Chem-REAS (r = 0.38) is higher than

GMDD
8, 9373–9413, 2015

that calculated for WRF-Chem-EDGAR ($r = 0.2$). In terms of bias, both simulations produce similar NMB and MFB for O_3. For PM_{10}, NO_2, and SO_2, WRF-Chem-REAS has a smaller MFB than WRF-Chem-EDGAR. In terms of error, MFE and NMSE from the two simulations are comparable for O_3 but WRF-Chem-REAS results in less MFE and NMSE for PM_{10} and NO_2. According to the model performance goals and criteria of PM_{10} suggested by Boylan and Russell (2006), WRF-Chem-EDGAR meets the performance criteria, while WRF-Chem-REAS achieves the stricter performance goals.

Based on the above performance analyses, we choose REAS as the anthropogenic emission inventory to conduct further simulations for four months to explore the seasonality of air pollutant concentrations. In this paper, we focus on validating the WRF-Chem model with REAS. More detailed comparisons, assessing the differences due to various inventories, will be conducted in our future work.

4 Spatiotemporal variations of pollutants and model evaluation

In this section, we analyze the spatial variability of simulated and observed monthly mean PM_{10} concentration, as well as O_3, SO_2, and NO_x mixing ratios (Figs. 4, 7, 9, and 10). A color-filled circle overlaid on a model-simulated monthly average surface concentration map represents the observed monthly-average value at each site. Tables 3–6 describe yearly statistics for PM_{10} concentrations, as well as O_3, SO_2, and NO_2 mixing ratios at individual stations, respectively. Table S5 summarizes seasonal statistics for the same pollutants at all available stations. The comparisons between daily modeled and observed concentrations of each pollutant are given in Figs. 5, 6, 8, and 11 for individual sites. Detailed analyses of model biases and errors for each of the species are provided in the following subsections.

4.1 PM_{10}

We obtain ground-level measurements from one site in Nepal, seven sites in Japan, and 71 sites in China. China is divided into seven geographical regions and measurements are analyzed, based on these regions (Table 3). The coverage of each geographical region in China is shown in Table S2. In China, the highest 4 month average PM_{10} is observed in the Northwest ($126 \pm 94\,\mu g\,m^{-3}$), followed by Northeast ($119 \pm 65\,\mu g\,m^{-3}$) and Central China ($117 \pm 48\,\mu g\,m^{-3}$), while the lowest observed PM_{10} is in South China ($82 \pm 28\,\mu g\,m^{-3}$). In Japan, the observed four month average PM_{10} concentration is $27 \pm 33\,\mu g\,m^{-3}$, which is more than three times lower than those observed in China.

The model simulates high PM_{10} concentrations (over $200\,\mu g\,m^{-3}$) near the Gobi Desert in Northwest China and in the border area near Iran, Afghanistan, and Pakistan (Fig. 4). In these areas, dust emissions are the predominant source of PM_{10} and the anthropogenic primary PM_{10} is negligible as shown in Fig. S1. Besides these areas, the model simulates high PM_{10} concentrations (up to $100\,\mu g\,m^{-3}$) over the North China Plain, the Yangtze River Delta region, and the Sichuan Basin. The model simulates relatively low PM_{10} concentrations (lower than $60\,\mu g\,m^{-3}$) in most of South, Southwest, and Northeast China, most of India, and other countries in the model domain. Unlike Northwest China, where the maximum PM_{10} concentrations are simulated in spring, other regions of China are simulated to have high concentrations in January and October, and low concentrations in April and July. This is because in winter reduced precipitation leads to higher PM_{10} concentrations, while the monsoon circulation brings in clean marine air and dilutes the PM_{10} surface concentrations in eastern China in summer. Moreover, aerosols in summer are removed by wet scavenging due to more frequent precipitation (Zhao et al., 2010). High concentrations are also simulated in an area surrounding Lhasa in Tibet in January. Since primary anthropogenic emissions in Tibet are low, dust emissions from local soils on the Plateau are the main reason for high PM_{10} concentrations. The previous study of tracer element analyses has shown

GMDD
8, 9373–9413, 2015

that local dust is the major source of total particulate matter (PM) over Tibet (Zhang et al., 2001).

For 4-month averaged PM_{10}, the model meets the performance criteria at 84 % of observation sites in China. The model tends to underestimate observations at the rest of the sites, which are mainly located in Northeast and Southwest China. Analyzing model–observation comparison by region, we find better model performance at Central, East, North, and South China (Table 3). However, Northeast and Southwest China have higher correlation ($r > 0.35$) than others. For sites outside of China, model underestimates observations in both Japan (MFB = −32 %) and Nepal (MFB = −48 %).

The seasonal statistics (Table S4) and Figs. 5–6 indicate that the model meets the performance criteria in all fourth months (January, April, July, and October) in Central, East, North and South China. In the remaining regions in China and Japan, model meets or is close to the criteria in April, July and October, but has more difficulty reproducing PM_{10} concentrations in January. Previous research has suggested that poor model performance in winter is common among air quality models and may be caused by difficulty in simulating stagnant weather conditions that lead to high winter PM concentrations (Tessum et al., 2015). In Nepal, model performance in both January and April is poor when the observed PM_{10} is high. The time series comparison plots (Fig. S2) reveal distinct air pollution episodes occurring in middle January and early April at the Godavari site, which the model fails to simulate. One of the possible reasons for this is that the model is unable to reproduce the local meteorology due to the complicated topography that is not well-resolved at the current horizontal resolution. The temporal correlations of all sites in each month are similar (0.37–0.39) as shown in Table S5 and we do not observe obvious trends of temporal correlations change with seasons.

4.2 O_3

Similar to PM_{10}, the simulated O_3 over the model domain also exhibits a seasonal variability that varies by region. Figure 7 illustrates that the highest O_3 mixing ratio (over

70 ppbv) occurs in North and East China in July. This is because biogenic NMVOC emissions are relatively high and active photochemical reactions constitute favorable conditions for the build-up of O_3 mixing ratios in summer. On the other hand, a low monthly mean mixing ratio (below 40 ppbv) is found in the same region in January. In the Tibetan Plateau, the surface O_3 mixing ratio reaches a maximum (over 70 ppbv) in April due to high elevations and downward transport of O_3 from the stratosphere, while the minimum O_3 (40 ppbv) is found in July because the upward transport of air to the stratosphere in the summer suppresses the downward transport of O_3 (Gettelman et al., 2004; Randel et al., 2010). This simulated seasonal variability of O_3 in our model over the Tibetan Plateau is consistent with the findings of Ma et al. (2014).

The Model performs well for simulating O_3 at all sites in Japan, and both MFB and MFE of these sites are within or close to the model benchmark (MFB $< \pm 15$ % and MFE < 35 %). The model overestimates O_3 at Lulin in Taiwan. MFB at Lulin (51 %) is more than twice higher than that of any sites in Japan and this may be because Lulin is a mountain site. Model reproduces the overall daily temporal variation of O_3 well ($r = 0.57$) and the value of temporal correlation is also high for each site (0.47–0.93) except at Rishiri. This is partly due to the lateral boundary conditions, since this site is located close to the northeast boundary of the model domain. The model predicts the seasonal variability well, as shown in Fig. 8 and Table S5. The modeled and observed monthly mean O_3 has a maximum in April and a minimum in July. The same seasonal characteristics of O_3 level were reported before (Yamaji et al., 2006). The MFB and MFE of all sites in each month are in the acceptable range. Among the four months, the model tends to underestimate the highest observations in April, while it overestimates observations in other three months.

4.3 SO_2 and NO_2

Figure 9 illustrates that the model simulates high monthly mean SO_2 mixing ratio (higher than 20 ppbv) over urban areas in North China (including Beijing, Tianjin, Hebei, and Shanxi), and some provinces in East China (including Shandong and Henan),

GMDD
8, 9373–9413, 2015

where emissions are also the highest. In these areas, the mixing ratios are the highest in January, followed by October, April, and July (Fig. 9). In winter, anthropogenic emissions are the highest because of extensive coal combustion particularly over northern China (Zhang et al., 2012). The lowest mixing ratios in our model simulation are found in July due to more active oxidation of SO_2 by hydroxyl radical (OH) and O_3 in the gas phase, as well as frequent precipitation that favors aqueous-phase oxidation of SO_2 (Feichter et al., 1996). Overall, the model predicts SO_2 well with MFB of 9 % and r of 0.64. The model performs better in predicting observed SO_2 mixing ratios at sites in Japan (MFB = −12–29 %, r = 0.52–0.82) than in China (MFB = −70 to 63 %, r = 0.14–0.5). The lowest overall MFB value of all sites occurs in April (8 %), while the highest happens in July (31 %). Although MFB values are acceptable, both MFE and NMSE in July and October are high. The site that contributes most to high errors is Beijing, with MFE of more than 115 % in these two months. The model largely overestimates SO_2 in Beijing (Fig. 11) probably because that the REAS emission inventory did not take into account the local emission control policies for the Beijing Olympics. In 2007, Chinese government reduced anthropogenic emissions by shutting down many polluting industries, banning high-emission vehicles, and restricting the number of on-road vehicles in Beijing (Zhang et al., 2012). It is likely that our emissions were overestimated in Beijing, which caused a large discrepancy between modeled and observed SO_2 mixing ratios.

The spatial and seasonal distribution of NO_2 is similar to SO_2 as shown in Fig. 10. High NO_2 mixing ratio is found over Northeast, North, and East China due to high emissions from power plant, industry and transportation sectors in these regions. Outside China, several hot spots are identified, such as Seoul (South Korea) and New Delhi (India). The modeled NO_2 mixing ratios have a summer minimum and a winter maximum. The lifetime of NO_2 in winter is relatively longer (18–24 h) than that in summer (6 h) because the concentration of hydroxyl radical (OH) in atmosphere is low (Beirle et al., 2003). Consequently, the removal reaction of NO_2 with OH radical to form HNO_3 is less active in winter than in summer. Among the four sites in China, the model performs well in predicting observed NO_2 mixing ratios at Shanghai (MFB = −9 %); however, it underestimates at the other three sites (MFB > −53 %). WRF-Chem captures the seasonal variability of NO_2, but underestimates the monthly average of NO_2 with MFB between −41 and −68 % for all four months. Underestimation of NO_2 was also been reported in the South Asian region using WRF-Chem (Kumar et al., 2012) and the possible reasons were proposed as the underestimation of NO_x emissions from biomass burning or anthropogenic sources. Another possible reason is that the removal of NO_x was overestimated through the heterogeneous reaction of N_2O_5 to form nitric acid in the WRF-Chem chemical mechanism RADM2 (Yegorova et al., 2011), used in this study.

5 Conclusions

We performed WRF-Chem simulation of air quality over East and South Asia using two different anthropogenic emission inventories and evaluated the model performance for PM_{10} concentrations, as well as O_3, SO_2, and NO_2 mixing ratios, using ground-level observations for the year 2007. We find that large discrepancies exist between the extensively-used EDGAR global anthropogenic emissions and the REAS regional inventory at national and provincial scales. The discrepancies between these inventories can lead to large differences in simulated surface PM_{10} concentrations (40–70 %), and moderate differences in O_3 mixing ratios (16–20 %) in most areas of North China Plain, as well as more than 100 % differences in SO_2 and NO_2 mixing ratios, found in several provinces in China. Our study demonstrates that WRF-Chem is sensitive to emissions inventories and improvements in emission inventories are important for accurately simulating regional air quality. Further studies are needed to assess model performance differences due to different emission inputs.

On the basis of lower bias and error values vs. observations we found for our REAS-driven simulations, we chose this inventory for use in four one-month simulations for the purpose of model evaluation. The model results indicate clear regional variations in the seasonal cycle of surface PM_{10} and O_3 over East and South Asia. In Northwest China, maximum PM_{10} occurs in April, while in Nepal and other regions of China, the

GMDD
8, 9373–9413, 2015
Air Quality Modeling with WRF-Chem v3.5 in East and South Asia
M. Zhong et al.

highest PM_{10} mainly occurs in January. For surface O_3 mixing ratios, the peak values are simulated in July for North and East China, and April for Tibet and Japan. Comparisons between model simulations and observations show that the model performs well in simulating surface PM_{10} and O_3, meeting air quality model performance criteria for both PM_{10} and O_3 at most sites, although the model underestimates PM_{10} at some sites in China in January. The model predicts SO_2 better at sites in Japan than in China, where overestimation is large at Beijing site in July and October. The mode underestimates most observed NO_2 in all four months. These findings suggest that future model development and evaluation of emission inventories and models are needed for particulate matter and gaseous pollutants in East and South Asia.

Code availability

The WRF-Chem model is an open-source, publicly available, and continually developed software. The version 3.5 used in this study can be downloaded at http://www2.mmm.ucar.edu/wrf/users/download/get_source.html. Known problems of the WRF-Chem version 3.5 have been fixed, using solutions provided online at http://ruc.noaa.gov/wrf/WG11/known-prob_v3.5.htm. We have optimized dust parameterizations in the code, using observed ground-level PM_{10} concentrations. The modified code can be obtained from the corresponding authors.

The Supplement related to this article is available online at doi:10.5194/gmdd-8-9373-2015-supplement.

Acknowledgements. The NCEP GFS data used for this study are from the Research Data Archive (RDA) which is maintained by the Computational and Information Systems Laboratory(CISL) at the National Center for Atmospheric Research (NCAR). The data is available at http://rda.ucar.edu/datasets/ds083.0/. We thank Keiichi SATO at the Asia Center for Air Pollution Research for providing EANET data. Ambient aerosol measurements in Godavari, Nepal were supported by Pradeep Dangol and Bidya Banmali Pradhan of the International Center for Integrated Mountain Development, James Schauer of the Unviersity of Wisconsin-Madison, and were funded through the United Nations Environmental Programme and the National Oceanic and Atmospheric Administration. This study was supported by the Energy Foundation (Grant number G-1208-16644) and the National Science Foundation (Grant number AGS-1350021). We gratefully acknowledge Songmiao Fan for providing constructive suggestions.

References

Ackermann, I. J., Hass, H., Memmesheimer, M., Ebel, A., Binkowski, F. S., and Shankar, U.: Modal aerosol dynamics model for Europe: development and first applications, Atmos. Environ., 32, 2981–2999, doi:10.1016/S1352-2310(98)00006-5, 1998. 9378

Amnuaylojaroen, T., Barth, M. C., Emmons, L. K., Carmichael, G. R., Kreasuwun, J., Prasitwattanaseree, S., and Chantara, S.: Effect of different emission inventories on modeled ozone and carbon monoxide in Southeast Asia, Atmos. Chem. Phys., 14, 12983–13012, doi:10.5194/acp-14-12983-2014, 2014. 9377

Beirle, S., Platt, U., Wenig, M., and Wagner, T.: Weekly cycle of NO_2 by GOME measurements: a signature of anthropogenic sources, Atmos. Chem. Phys., 3, 2225–2232, doi:10.5194/acp-3-2225-2003, 2003. 9388

Binkowski, F. S. and Shankar, U.: The regional particulate matter model: 1. model description and preliminary results, J. Geophys. Res., 100, 26191–26209, doi:10.1029/95JD02093, 1995. 9379

Boylan, J. W. and Russell, A. G.: PM and light extinction model performance metrics, goals, and criteria for three-dimensional air quality models, Atmos. Environ., 40, 4946–4959, doi:10.1016/j.atmosenv.2005.09.087, 2006. 9381, 9384

Chapman, E. G., Gustafson Jr., W. I., Easter, R. C., Barnard, J. C., Ghan, S. J., Pekour, M. S., and Fast, J. D.: Coupling aerosol-cloud-radiative processes in the WRF-Chem model: Investigating the radiative impact of elevated point sources, Atmos. Chem. Phys., 9, 945–964, doi:10.5194/acp-9-945-2009, 2009. 9379

Chen, Z., Wang, J.-N., Ma, G.-X., and Zhang, Y.-S.: China tackles the health effects of air pollution, The Lancet, 382, 1959–1960, available at: http://linkinghub.elsevier.com/retrieve/pii/S0140673613620644 (last access: 15 November 2014), 2013. 9376

Colette, A., Bessagnet, B., Vautard, R., Szopa, S., Rao, S., Schucht, S., Klimont, Z., Menut, L., Clain, G., Meleux, F., Curci, G., and Rouïl, L.: European atmosphere in 2050, a regional air quality and climate perspective under CMIP5 scenarios, Atmos. Chem. Phys., 13, 7451–7471, doi:10.5194/acp-13-7451-2013, 2013. 9380

Donner, L. J., Wyman, B. L., Hemler, R. S., Horowitz, L. W., Ming, Y., Zhao, M., Golaz, J.-C., Ginoux, P., Lin, S. J., Schwarzkopf, M. D., Austin, J., Alaka, G., Cooke, W. F., Delworth, T. L., Freidenreich, S. M., Gordon, C. T., Griffies, S. M., Held, I. M., Hurlin, W. J., Klein, S. A., Knutson, T. R., Langenhorst, A. R., Lee, H.-C., Lin, Y., Magi, B. I., Malyshev, S. L., Milly, P. C. D., Naik, V., Nath, M. J., Pincus, R., Ploshay, J. J., Ramaswamy, V., Seman, C. J., Shevliakova, E., Sirutis, J. J., Stern, W. F., Stouffer, R. J., Wilson, R. J., Winton, M., Wittenberg, A. T., and Zeng, F.: The dynamical core, physical parameterizations, and basic simulation characteristics of the atmospheric component AM3 of the GFDL Global Coupled Model CM3, J. Climate, 24, 3484–3519, doi:10.1175/2011JCLI3955.1, 2011. 9379

Easter, R. C., Ghan, S. J., Zhang, Y., Saylor, R. D., Chapman, E. G., Laulainen, N. S., Abdul-Razzak, H., Leung, L. R., Bian, X., and Zaveri, R. A.: MIRAGE: Model description and evaluation of aerosols and trace gases, J. Geophys. Res., 109, D20210, doi:10.1029/2004JD004571, 2004. 9379

Feichter, J., Kjellström, E., Rodhe, H., Dentener, F., Lelieveldi, J., and Roelofs, G.-J.: Simulation of the tropospheric sulfur cycle in a global climate model, Atmos. Environ., 30, 1693–1707, doi:10.1016/1352-2310(95)00394-0, 1996. 9388

Fry, M. M., Naik, V., West, J. J., Schwarzkopf, M. D., Fiore, A. M., Collins, W. J., Dentener, F. J., Shindell, D. T., Atherton, C., Bergmann, D., Duncan, B. N., Hess, P., MacKenzie, I. A., Marmer, E., Schultz, M. G., Szopa, S., Wild, O., and Zeng, G.: The influence of ozone precursor emissions from four world regions on tropospheric composition and radiative climate forcing, J. Geophys. Res., 117, D07306, doi:10.1029/2011JD017134, 2012. 9380

Gao, Y., Fu, J. S., Drake, J. B., Lamarque, J. F., and Liu, Y.: The impact of emission and climate change on ozone in the United States under representative concentration pathways (RCPs), Atmos. Chem. Phys., 13, 9607–9621, doi:10.5194/acp-13-9607-2013, 2013. 9380

Gao, Y., Zhao, C., Liu, X., Zhang, M., and Leung, L. R.: WRF-Chem simulations of aerosols and anthropogenic aerosol radiative forcing in East Asia, Atmos. Environ., 92, 250–266, doi:10.1016/j.atmosenv.2014.04.038, 2014. 9377, 9379

Gettelman, A., Kinnison, D. E., Dunkerton, T. J., and Brasseur, G. P.: Impact of monsoon circulations on the upper troposphere and lower stratosphere, J. Geophys. Res., 109, D22101, doi:10.1029/2004JD004878, 2004. 9387

Gong, S. L.: A parameterization of sea-salt aerosol source function for sub- and super-micron particles, Global Biogeochem. Cy., 17, 1097, doi:10.1029/2003GB002079, 2003. 9380

Granier, C., Lamarque, J. F., Mieville, A., Muller, J. F., Olivier, J., Orlando, J., Peters, J., Petron, G., Tyndall, G., and Wallens, S.: POET, a database of surface emissions of ozone precursors, available at: http://www.aero.jussieu.fr/projet/ACCENT/POET.php (last access: 25 October 2013), 2005. 9380

Grell, G. A. and Dévényi, D.: A generalized approach to parameterizing convection combining ensemble and data assimilation techniques, Geophys. Res. Lett., 29, 38-1–38-4, doi:10.1029/2002GL015311, 2002. 9379

Grell, G. A., Peckham, S. E., Schmitz, R., McKeen, S. A., Frost, G., Skamarock, W. C., and Eder, B.: Fully coupled “online” chemistry within the WRF model, Atmos. Environ., 39, 6957–6975, doi:10.1016/j.atmosenv.2005.04.027, 2005. 9376, 9378

HEI: Outdoor air pollution among top global health risks in 2010, available at: http://www.healtheffects.org/International/HEI-India-GBD-PressRelease021313.pdf (last access: 20 May 2014), 2013. 9376

John, J. G., Fiore, A. M., Naik, V., Horowitz, L. W., and Dunne, J. P.: Climate versus emission drivers of methane lifetime against loss by tropospheric OH from 1860–2100, Atmos. Chem. Phys., 12, 12021–12036, doi:10.5194/acp-12-12021-2012, 2012. 9379

JRC and PBL: Emission Database for Global Atmospheric Research (EDGAR), version 4.2., European Commission, Joint Research Centre/PBL Netherlands Environmental Assessment Agency, available at: http://edgar.jrc.ec.europa.eu (last access: 19 March 2014), 2010. 9377, 9383

Kumar, R., Naja, M., Pfister, G. G., Barth, M. C., Wiedinmyer, C., and Brasseur, G. P.: Simulations over South Asia using the Weather Research and Forecasting model with Chemistry (WRF-Chem): chemistry evaluation and initial results, Geosci. Model Dev., 5, 619–648, doi:10.5194/gmd-5-619-2012, 2012. 9376, 9379, 9389

Kurokawa, J., Ohara, T., Morikawa, T., Hanayama, S., Janssens-Maenhout, G., Fukui, T., Kawashima, K., and Akimoto, H.: Emissions of air pollutants and greenhouse gases over Asian regions during 2000–2008: Regional Emission inventory in ASia (REAS) version 2, Atmos. Chem. Phys., 13, 11019–11058, doi:10.5194/acp-13-11019-2013, 2013. 9377, 9380, 9383

Lin, Y.-L., Farley, R. D., and Orville, H. D.: Bulk parameterization of the snow field in a cloud model, J. Clim. Appl. Meteorol., 22, 1065–1092, doi:10.1175/1520-0450(1983)022<1065:BPOTSF>2.0.CO;2, 1983. 9379

Liu, X.-H., Zhang, Y., Cheng, S.-H., Xing, J., Zhang, Q., Streets, D. G., Jang, C., Wang, W.-X., and Hao, J.-M.: Understanding of regional air pollution over China using CMAQ, part I performance evaluation and seasonal variation, Atmos. Environ., 44, 2415–2426, doi:10.1016/j.atmosenv.2010.03.035, 2010. 9381

Ma, J. and van Aardenne, J. A.: Impact of different emission inventories on simulated tropospheric ozone over China: a regional chemical transport model evaluation, Atmos. Chem. Phys., 4, 877–887, doi:10.5194/acp-4-877-2004, 2004. 9377

Ma, J., Lin, W. L., Zheng, X. D., Xu, X. B., Li, Z., and Yang, L. L: Influence of air mass downward transport on the variability of surface ozone at Xianggelila Regional Atmosphere Background Station, southwest China, Atmos. Chem. Phys., 14, 5311–5325, doi:10.5194/acp-14-5311-2014, 2014. 9387

Morris, R., Koo, B., McNally, D., Tesche, T., and Tonnesen, G.: Application of multiple models to simulation fine particulate in the Southeastern US, presented at the National Regional Planning Organizations Modeling Meeting, Denver, CO, 2005. 9382

Naik, V., Horowitz, L. W., Fiore, A. M., Ginoux, P., Mao, J., Aghedo, A. M., and Levy, H.: Impact of preindustrial to present-day changes in short-lived pollutant emissions on atmospheric composition and climate forcing, J. Geophys. Res., 118, 8086–8110, doi:10.1002/jgrd.50608, 2013. 9379

Ou Yang, C.-F., Lin, N.-H., Sheu, G.-R., Lee, C.-T., and Wang, J.-L.: Seasonal and diurnal variations of ozone at a high-altitude mountain baseline station in East Asia, Atmos. Environ., 46, 279–288, doi:10.1016/j.atmosenv.2011.09.060, 2012. 9381

Qu, W. J., Arimoto, R., Zhang, X. Y., Zhao, C. H., Wang, Y. Q., Sheng, L. F., and Fu, G.: Spatial distribution and interannual variation of surface PM_{10} concentrations over eighty-six Chinese cities, Atmos. Chem. Phys., 10, 5641–5662, doi:10.5194/acp-10-5641-2010, 2010. 9381

Ramanathan, V., Li, F., Ramana, M. V., Praveen, P. S., Kim, D., Corrigan, C. E., Nguyen, H., Stone, E. A., Schauer, J. J., Carmichael, G. R., Adhikary, B., and Yoon, S. C.: Atmospheric brown clouds: hemispherical and regional variations in long-range transport, absorption, and radiative forcing, J. Geophys. Res., 112, D22S21, doi:10.1029/2006JD008124, 2007. 9381

GMDD

8, 9373–9413, 2015

Air Quality Modeling with WRF-Chem v3.5 in East and South Asia

M. Zhong et al.

Randel, W. J., Park, M., Emmons, L., Kinnison, D., Bernath, P., Walker, K. A., Boone, C., and Pumphrey, H.: Asian Monsoon transport of pollution to the stratosphere, Science, 328, 611–613, doi:10.1126/science.1182274, 2010. 9387

Randerson, J., van der Werf, G., Giglio, L., Collatz, G., and Kasibhatla, P.: Global Fire Emissions Database, Version 3 (GFEDv3.1), doi:10.3334/ORNLDAAC/1191, 2013. 9380

Riahi, K., Rao, S., Krey, V., Cho, C., Chirkov, V., Fischer, G., Kindermann, G., Nakicenovic, N., and Rafaj, P.: RCP 8.5 – a scenario of comparatively high greenhouse gas emissions, Climatic Change, 109, 33–57, doi:10.1007/s10584-011-0149-y, 2011. 9380

Saikawa, E., Kurokawa, J., Takigawa, M., Borken-Kleefeld, J., Mauzerall, D. L., Horowitz, L. W., and Ohara, T.: The impact of China's vehicle emissions on regional air quality in 2000 and 2020: a scenario analysis, Atmos. Chem. Phys., 11, 9465–9484, doi:10.5194/acp-11-9465-2011, 2011. 9376, 9377, 9379

Schell, B., Ackermann, I. J., Hass, H., Binkowski, F. S., and Ebel, A.: Modeling the formation of secondary organic aerosol within a comprehensive air quality model system, J. Geophys. Res., 106, 28275–28293, 2001. 9378

Seinfeld, J. H. and Pandis, S. N.: Atmospheric Chemistry and Physics: From Air Pollution to Climate Change, John Wiley and Sons, New York, 2012. 9376

Shaw, W. J., Jerry Allwine, K., Fritz, B. G., Rutz, F. C., Rishel, J. P., and Chapman, E. G.: An evaluation of the wind erosion module in DUSTRAN, Atmos. Environ., 42, 1907–1921, doi:10.1016/j.atmosenv.2007.11.022, 2008. 9380

Stockwell, W. R., Middleton, P., Chang, J. S., and Tang, X.: The second generation regional acid deposition model chemical mechanism for regional air quality modeling, J. Geophys. Res., 95, 16343–16367, doi:10.1029/JD095iD10p16343, 1990. 9378

Stone, E. A., Schauer, J. J., Pradhan, B. B., Dangol, P. M., Habib, G., Venkataraman, C., and Ramanathan, V.: Characterization of emissions from South Asian biofuels and application to source apportionment of carbonaceous aerosol in the Himalayas, J. Geophys. Res., 115, D06301, doi:10.1029/2009JD011881, 2010. 9381

Tessum, C. W., Hill, J. D., and Marshall, J. D.: Twelve-month, 12 km resolution North American WRF-Chem v3.4 air quality simulation: performance evaluation, Geosci. Model Dev., 8, 957–973, doi:10.5194/gmd-8-957-2015, 2015. 9386

Tuccella, P., Curci, G., Visconti, G., Bessagnet, B., Menut, L., and Park, R. J.: Modeling of gas and aerosol with WRF/Chem over Europe: Evaluation and sensitivity study, J. Geophys. Res., 117, D03303, doi:10.1029/2011JD016302, 2012. 9379

Wang, K., Zhang, Y., Jang, C., Phillips, S., and Wang, B.: Modeling intercontinental air pollution transport over the trans-Pacific region in 2001 using the Community Multiscale Air Quality modeling system, J. Geophys. Res., 114, D04307, doi:10.1029/2008JD010807, 2009. 9381
Wang, X., Liang, X.-Z., Jiang, W., Tao, Z., Wang, J. X. L., Liu, H., Han, Z., Liu, S., Zhang, Y., Grell, G. A., and Peckham, S. E.: WRF-Chem simulation of East Asian air quality: Sensitivity to temporal and vertical emissions distributions, Atmos. Environ., 44, 660–669, doi:10.1016/j.atmosenv.2009.11.011, 2010. 9376
WHO: Ambient Air Pollution Database, available at: http://www.who.int/entity/quantifying_ehimpacts/national/countryprofile/AAP_PM_database_May2014.xls?ua=1, last access: 19 November 2014. 9376
Wild, O., Zhu, X., and Prather, M.: Fast-J: accurate simulation of in- and below-cloud photolysis in tropospheric chemical models, J. Atmos. Chem., 37, 245–282, doi:10.1023/A:1006415919030, 2000. 9379
Yamaji, K., Ohara, T., Uno, I., Tanimoto, H., Kurokawa, J.-I., and Akimoto, H.: Analysis of the seasonal variation of ozone in the boundary layer in East Asia using the Community Multiscale Air Quality model: What controls surface ozone levels over Japan?, Atmos. Environ., 40, 1856–1868, doi:10.1016/j.atmosenv.2005.10.067, 2006. 9387
Yegorova, E. A., Allen, D. J., Loughner, C. P., Pickering, K. E., and Dickerson, R. R.: Characterization of an eastern U.S. severe air pollution episode using WRF/Chem, J. Geophys. Res., 116, D17306, doi:10.1029/2010JD015054, 2011. 9389
Zhang, X., van Geffen, J., Liao, H., Zhang, P., and Lou, S.: Spatiotemporal variations of tropospheric SO_2 over China by SCIAMACHY observations during 2004–2009, Atmos. Environ., 60, 238–246, doi:10.1016/j.atmosenv.2012.06.009, 2012. 9388
Zhang, X. Y., Arimoto, R., Cao, J. J., An, Z. S., and Wang, D.: Atmospheric dust aerosol over the Tibetan Plateau, J. Geophys. Res., 106, 18471–18476, doi:10.1029/2000JD900672, 2001. 9386
Zhao, C., Wang, Y., Yang, Q., Fu, R., Cunnold, D., and Choi, Y.: Impact of East Asian summer monsoon on the air quality over China: view from space, J. Geophys. Res., 115, D09301, doi:10.1029/2009JD012745, 2010. 9385

Table 1. List of total emissions for major pollutants from REAS and EDGAR over the model domain in July 2007. Unit is $Tg\,month^{-1}$.

Emission Inventory	PM_{10}	CO	SO_2	NO_x	NMVOCs	NH_3
REAS	2.73	25.05	4.62	4.61	3.67	2.61
EDGAR	3.07	21.25	4.62	3.33	4.56	1.70

GMDD
8, 9373–9413, 2015

Table 2. Statistical measures calculated for model simulations using REAS and EDGAR as emissions inputs for PM_{10}, O_3, SO_2, and NO_2. r is correlation coefficient between observations and model simulations; NMB (%) is the normalized mean bias between observations and model simulations; MFB (%) and MFE (%) are the mean fractional bias and mean fractional error; NMSE is the normalized mean square error between observations and model.

Pollutant	REAS					EDGAR				
	r	NMB	MFB	MFE	NMSE	r	NMB	MFB	MFE	NMSE
PM_{10}	0.38	−2.04	−11.49	46.42	0.36	0.20	−27.28	−37.34	56.70	0.58
O_3	0.83	19.11	24.50	30.95	0.10	0.82	19.20	25.24	32.33	0.10
SO_2	0.72	138.64	51.60	84.93	3.58	0.64	98.42	70.38	94.09	2.03
NO_2	0.68	−18.32	−22.50	50.98	0.41	0.66	−59.88	−71.52	83.05	1.57

GMDD
8, 9373–9413, 2015

Table 3. Statistical measures for model performance evaluation for PM_{10} for the year 2007. Count is the total number of observations for calculation; Obs ($\mu g\,m^{-3}$) and Model ($\mu g\,m^{-3}$) are 4-month mean daily average value of observations and model simulations, respectively. Other indicators and associated units are described in Table 2.

Region	Count	Obs	Model	r	NMB	MFB	MFE	NMSE
Central China	726	117.45	114.21	0.32	−2.75	−5.23	40.47	0.25
East China	1908	103.05	102.41	0.28	−0.63	−3.85	38.05	0.31
North China	1068	116.35	105.35	0.30	−9.45	−11.52	43.65	0.39
Northeast China	826	119.07	87.83	0.39	−26.24	−41.15	61.26	0.59
Northwest China	462	126.86	105.80	0.13	−16.60	−16.54	53.39	0.95
South China	452	82.74	68.97	0.18	−16.64	−22.27	44.68	0.31
Japan	409	25.44	20.83	0.27	−18.10	−32.34	65.24	2.00
Nepal	89	49.63	21.15	0.29	−57.38	−47.89	75.07	2.10
All sites	6874	102.46	89.15	0.39	−12.99	−19.95	48.40	0.46

GMDD
8, 9373–9413, 2015

Table 4. Statistical measures for model performance evaluation for O_3 for the year 2007. The unit of Obs and Model is ppbv. Other statistical indicators and associated units are described in Table 2.

Location	Sites	Count	Obs	Model	r	NMB	MFB	MFE	NMSE
Japan	Happo	81	61.04	55.57	0.55	−8.95	−7.30	20.57	0.06
	Hedo	90	39.59	45.79	0.93	15.68	20.60	22.42	0.04
	Oki	99	43.72	50.19	0.60	14.81	16.01	20.18	0.06
	Rishiri	54	47.14	46.12	0.03	−2.16	−0.92	15.41	0.03
	Sado-seki	82	46.24	47.85	0.61	3.48	4.59	12.13	0.02
	Tappi	101	51.75	45.95	0.56	−11.21	−9.84	17.65	0.05
	Yusuhara	102	42.80	47.68	0.75	11.40	12.75	17.31	0.04
Taiwan	Lulin	103	28.00	45.49	0.46	62.43	51.47	53.97	0.36
All sites		712	44.45	48.03	0.63	8.05	12.34	23.34	0.08

GMDD
8, 9373–9413, 2015

Air Quality Modeling with WRF-Chem v3.5 in East and South Asia

M. Zhong et al.

Table 5. Statistical measures for model performance evaluation for SO_2 for the year 2007. The unit of Obs and Model is ppbv. Other statistical indicators and associated units are described in Table 2.

Location	Sites	Count	Obs	Model	r	NMB	MFB	MFE	NMSE
Japan	Happo	65	0.60	0.72	0.53	19.27	20.96	77.56	1.23
	Hedo	86	0.51	0.37	0.66	−27.57	−12.17	69.44	1.70
	Oki	89	0.85	0.82	0.52	−3.60	29.31	69.73	1.77
	Rishiri	50	0.23	0.22	0.71	−2.90	17.84	55.33	0.46
	Tappi	97	0.43	0.37	0.65	−13.66	−1.71	51.61	0.78
	Yusuhara	99	1.27	1.26	0.82	−0.59	26.55	63.58	0.72
China	Xiamen	122	11.79	4.90	0.14	−58.42	−70.79	81.26	1.62
	Jinyunshan	123	10.10	17.81	0.50	76.34	62.19	75.48	0.85
	Zhuhai	123	6.88	8.16	0.29	18.74	5.27	52.50	0.67
	Beijing	123	15.65	21.74	0.32	38.92	63.38	91.86	1.05
	Shanghai	123	22.71	30.57	0.38	34.57	20.10	51.59	0.56
All sites		1100	7.80	8.82	0.64	13.06	8.89	65.80	1.52

GMDD
8, 9373–9413, 2015

Air Quality Modeling with WRF-Chem v3.5 in East and South Asia

M. Zhong et al.

Table 6. Statistical measures for model performance evaluation for NO_2 for the year 2007. The unit of Obs and Model is ppbv. Other statistical indicators and associated units are described in Table 2.

Location	Sites	Count	Obs	Model	r	NMB	MFB	MFE	NMSE
China	Beijing	123	32.17	18.63	0.47	−42.09	−53.69	58.67	0.48
	Shanghai	123	29.45	30.57	0.21	3.81	−9.26	46.65	0.41
	Jinyunshan	123	7.04	2.82	0.34	−59.89	−74.42	87.77	2.16
	Zhuhai	123	19.42	7.97	0.11	−58.95	−82.08	86.11	1.34
All sites		492	36.78	15.00	0.56	−31.88	−54.86	69.80	0.69

GMDD
8, 9373–9413, 2015

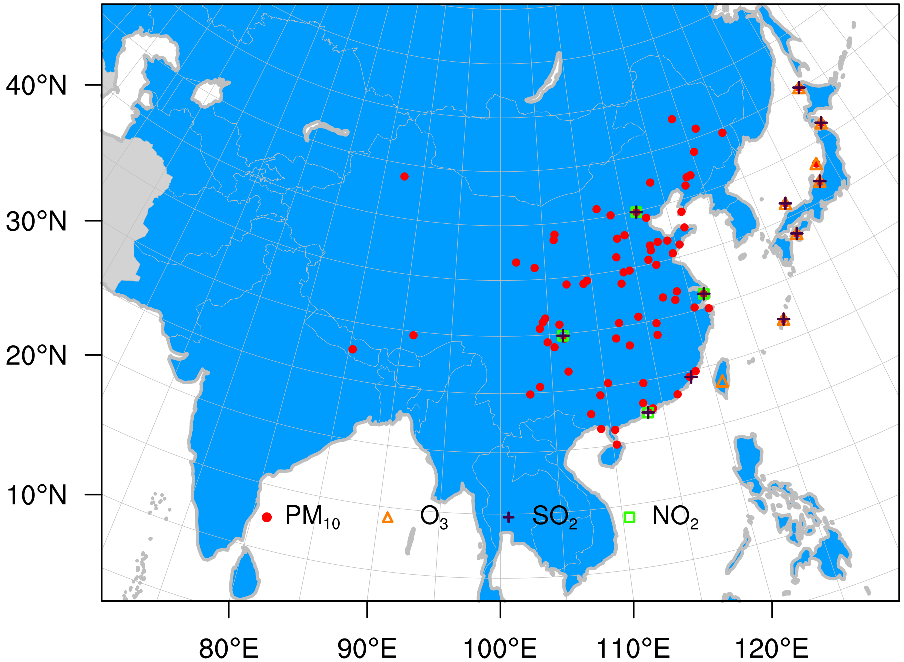

Figure 1. WRF-Chem model domain and observation sites. Blue shading indicates locations where the REAS emission inventory is used. Gray shading indicates where the RCP8.5 emissions are used. For the entire model domain, biomass burning emissions from GFED v3 and biogenic emissions from POET v1 are used. Red-filled circles denote the observational sites with PM_{10}; orange triangles for sites with O_3; purple crosses for sites with SO_2; and green squares for sites with NO_2.

GMDD
8, 9373–9413, 2015

Air Quality Modeling with WRF-Chem v3.5 in East and South Asia

M. Zhong et al.

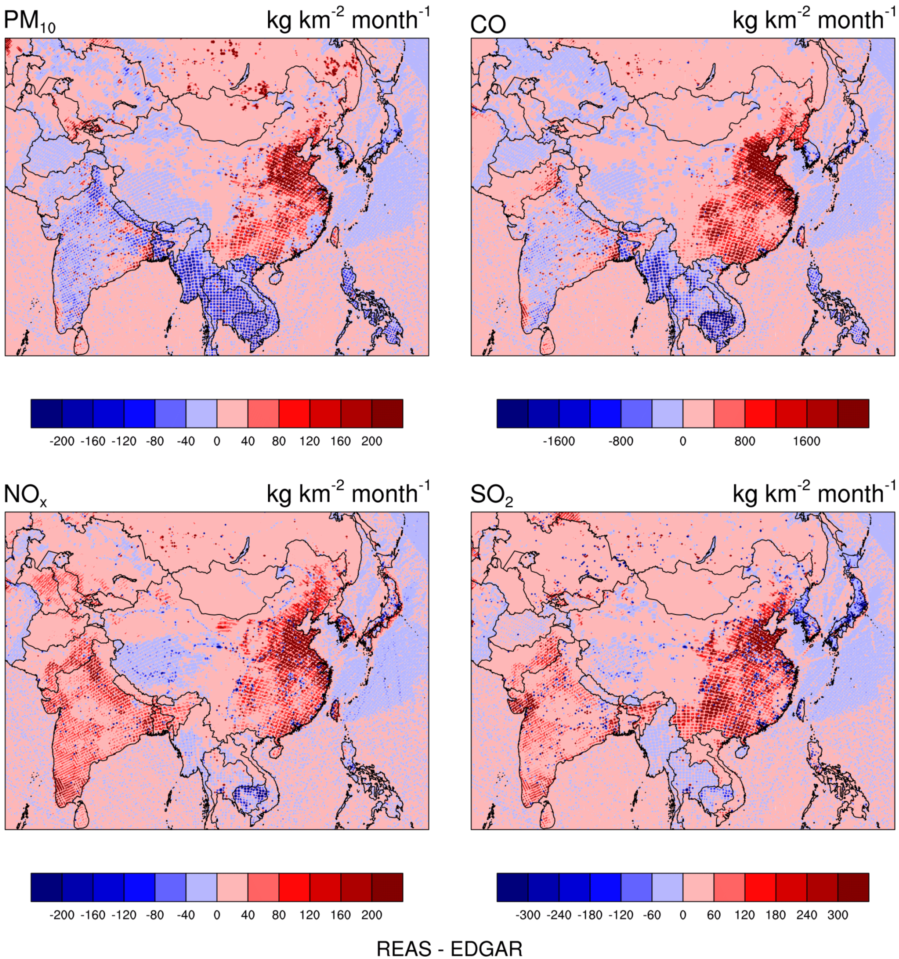

Figure 2. Monthly emissions difference of PM_{10}, CO, SO_2, and NO_x between REAS and EDGAR in July 2007 in our model domain.

GMDD
8, 9373–9413, 2015

Air Quality Modeling with WRF-Chem v3.5 in East and South Asia

M. Zhong et al.

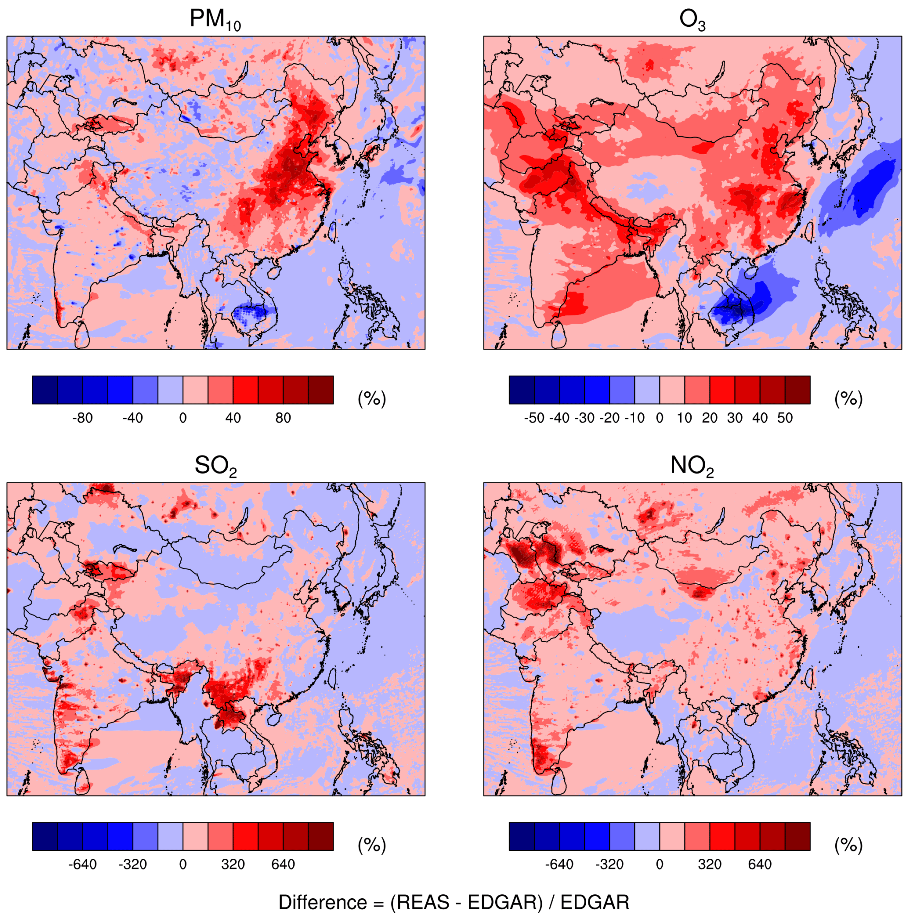

Figure 3. Percentage difference of 14-day mean PM_{10}, O_3, SO_2, and NO_2, between WRF-Chem simulations with REAS emissions (WRF-Chem-REAS) and EDGAR emissions (WRF-Chem-EDGAR).

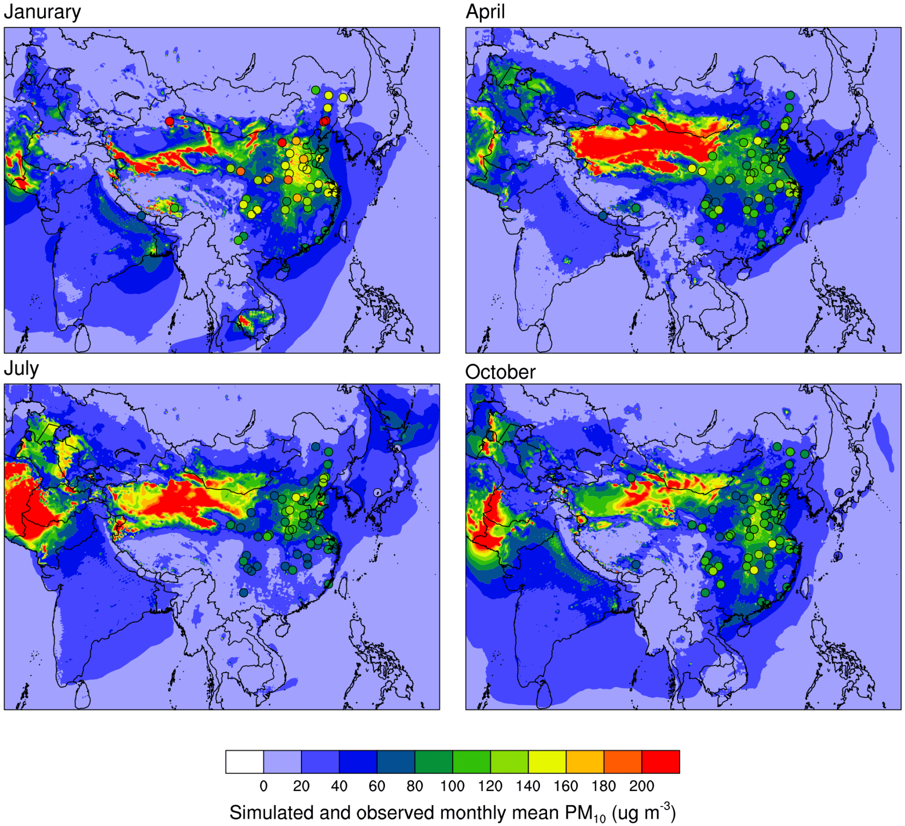

Figure 4. Simulated and observed monthly average surface PM_{10} in 2007 using WRF-Chem-REAS. The filled circles indicate the observed monthly average values.

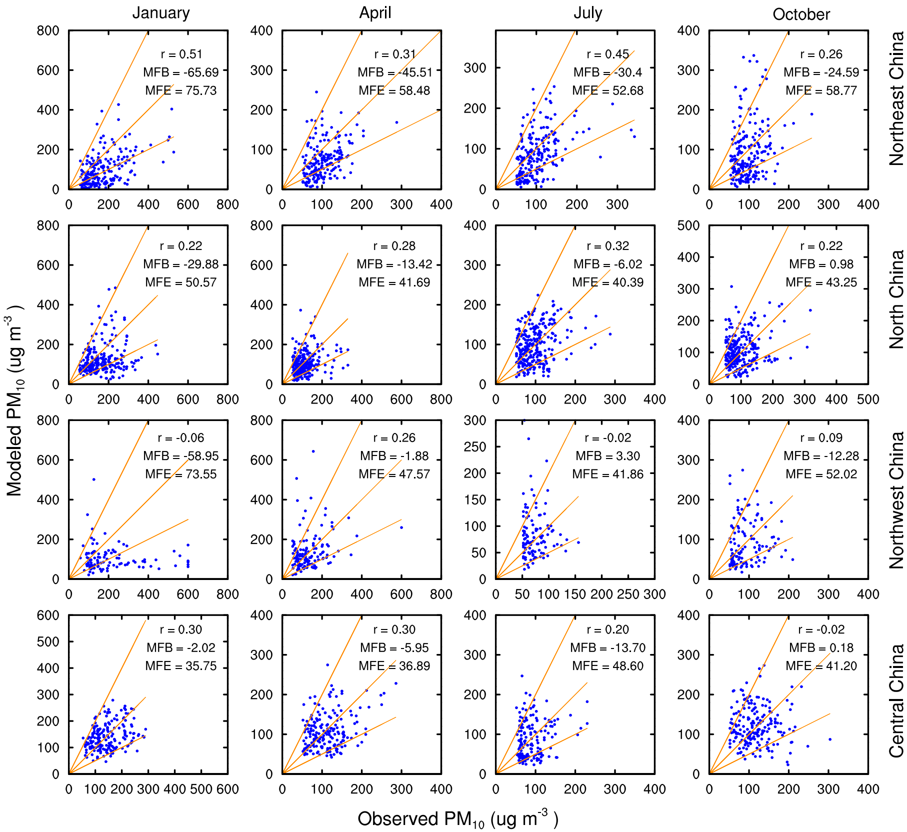

Figure 5. Comparisons of simulated and observed daily mean PM_{10} ($\mu g\,m^{-3}$) at Northeast, North, Northwest, and Central China in each month. The model to observation ratios of 2 : 1, 1 : 1, and 1 : 2 are represented in orange lines. Monthly average performance statistics (r, MFB, and MFE) are listed.

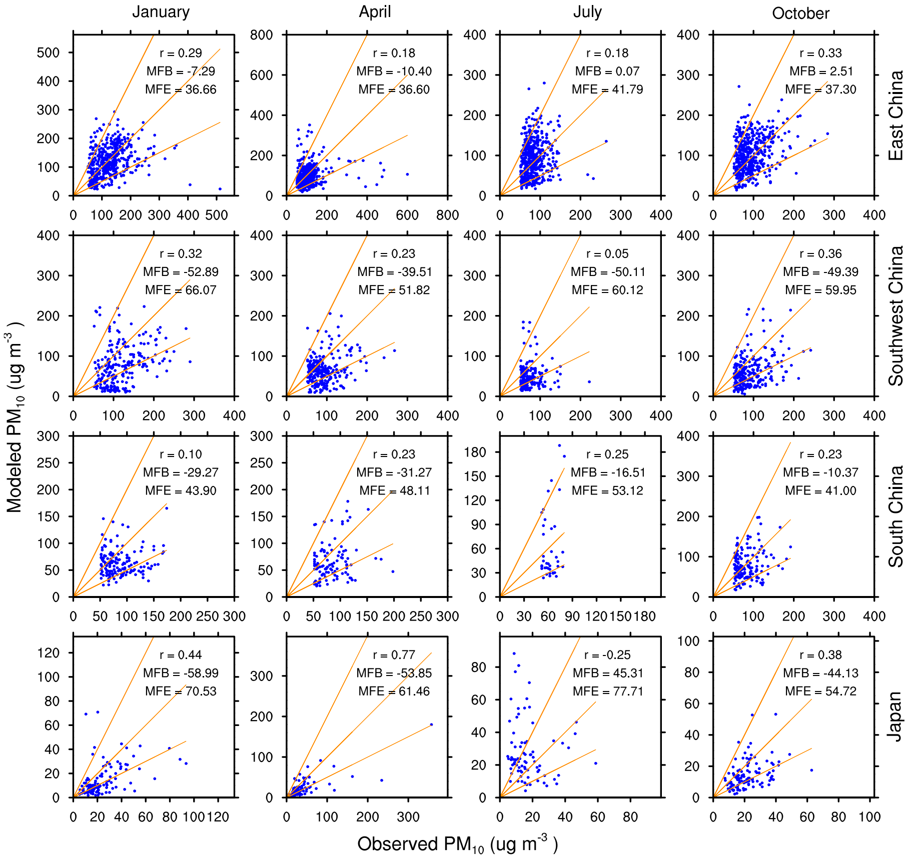

Figure 6. Comparisons of simulated and observed daily mean PM_{10} ($\mu g\,m^{-3}$) at East, Southwest, South region in China, and Japan in each month. The model to observation ratios of 2 : 1, 1 : 1, and 1 : 2 are represented in orange lines. Monthly average performance statistics (*r*, MFB, and MFE) are listed.

GMDD
8, 9373–9413, 2015

Air Quality Modeling with WRF-Chem v3.5 in East and South Asia

M. Zhong et al.

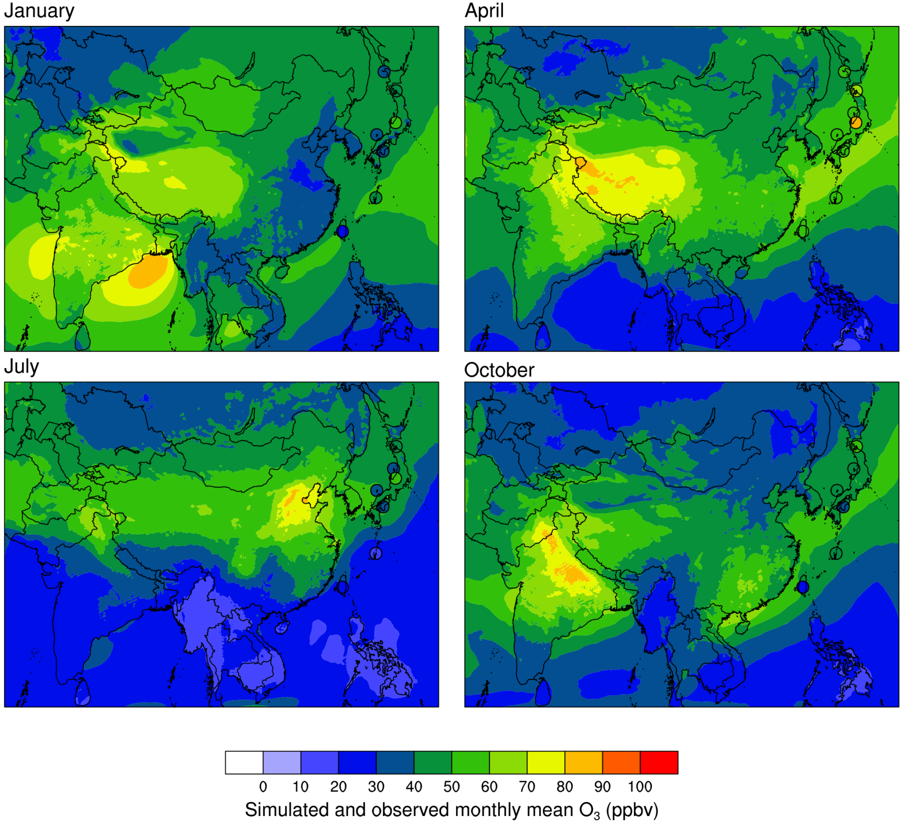

Figure 7. Simulated and observed monthly average surface O_3 in 2007 using WRF-Chem-REAS. The filled circles indicate the observed monthly average values.

GMDD
8, 9373–9413, 2015

Title Page
Abstract Introduction
Conclusions References
Tables Figures
◀ ▶
Back Close
Full Screen / Esc
Printer-friendly Version
Interactive Discussion

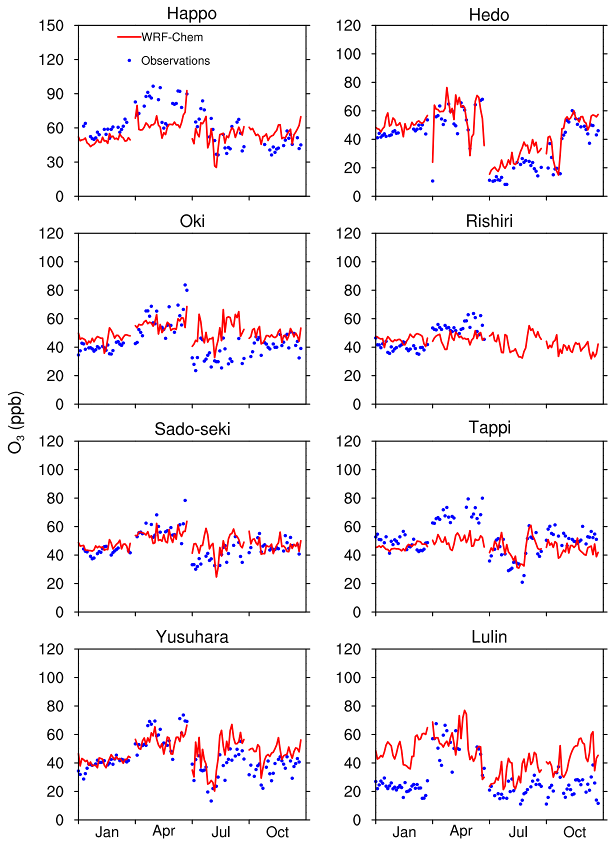

Figure 8. Comparisons of observed (blue dots) and modeled (red lines) daily mean O_3 (ppbv) at seven sites in Japan and one site in Taiwan.

GMDD
8, 9373–9413, 2015

Air Quality Modeling with WRF-Chem v3.5 in East and South Asia

M. Zhong et al.

Title Page
Abstract
Introduction
Conclusions
References
Tables
Figures
◄
►
Back
Close
Full Screen / Esc
Printer-friendly Version
Interactive Discussion

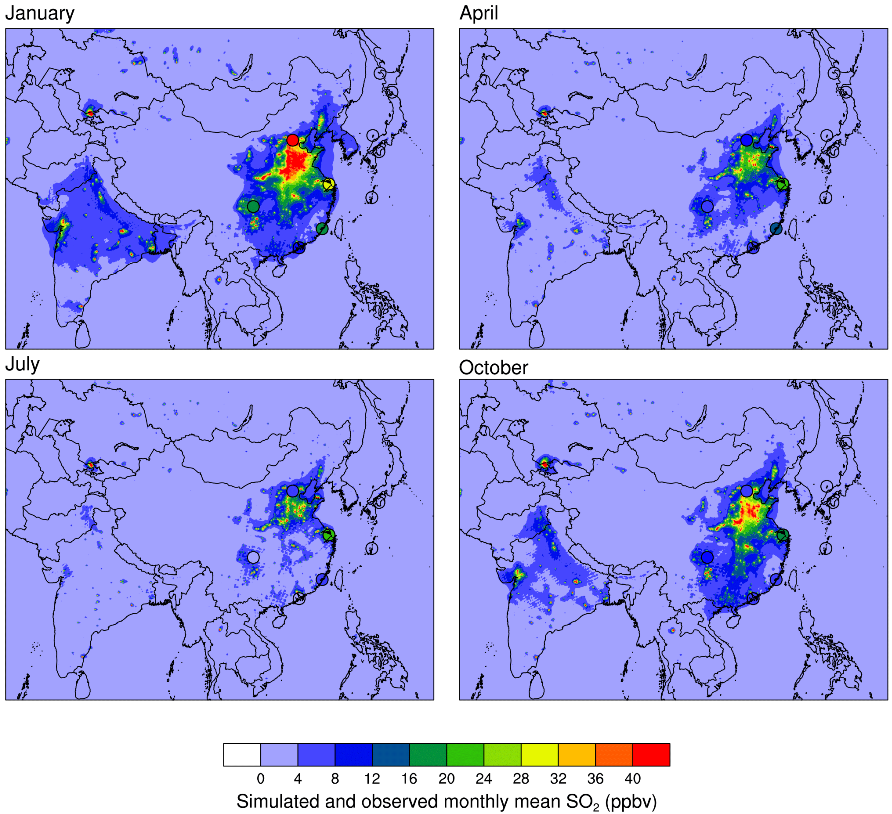

Figure 9. Simulated and observed monthly average surface SO_2 in 2007 using WRF-Chem-REAS. The filled circles indicate the observed monthly average values.

GMDD
8, 9373–9413, 2015

Air Quality Modeling with WRF-Chem v3.5 in East and South Asia

M. Zhong et al.

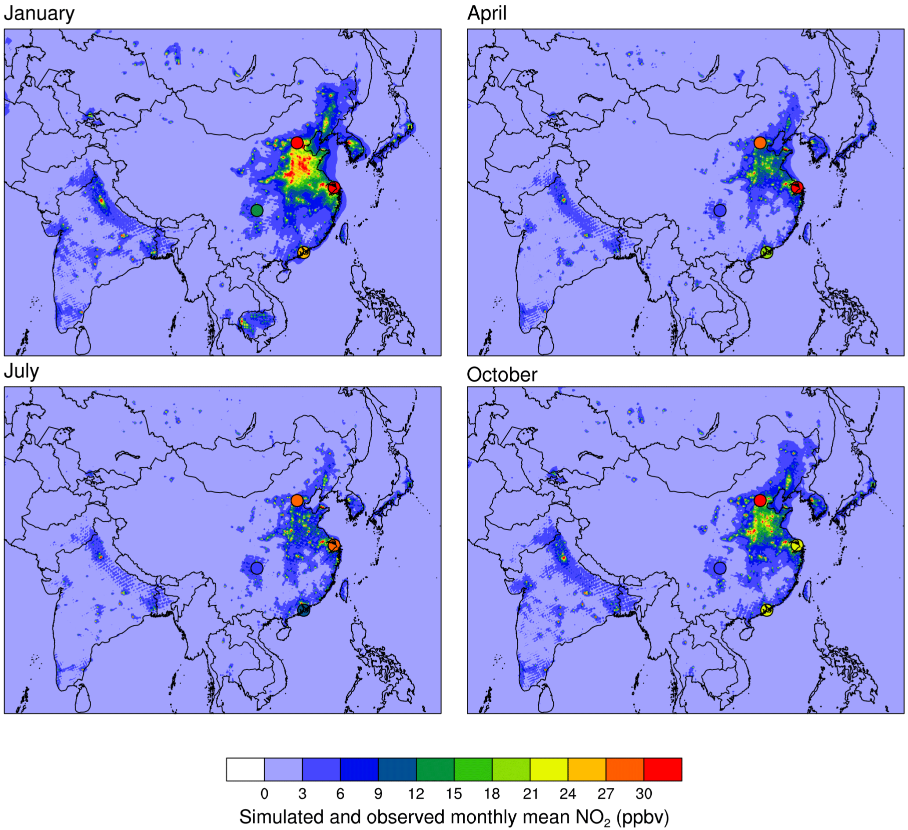

Figure 10. Simulated and observed monthly average surface NO_2 in 2007 using WRF-Chem-REAS. The filled circles indicate the observed monthly average values.

GMDD
8, 9373–9413, 2015

Air Quality Modeling with WRF-Chem v3.5 in East and South Asia

M. Zhong et al.

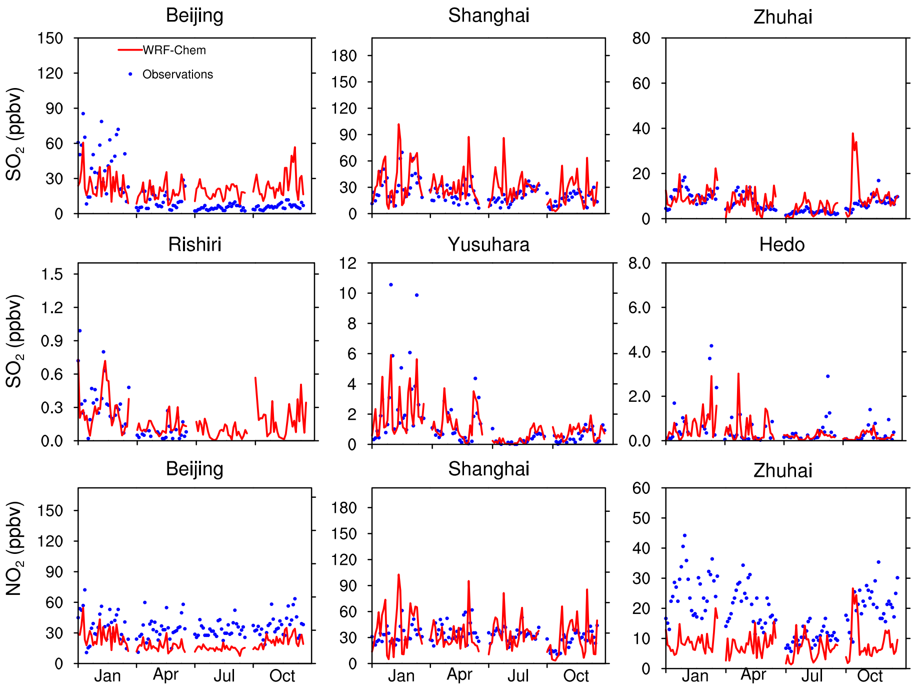

Figure 11. Comparisons of observed (blue dots) and modeled (red lines) daily mean SO_2 (ppbv) at six sites and NO_2 (ppbv) at three sites in China.

GMDD
8, 9373–9413, 2015

Air Quality Modeling with WRF-Chem v3.5 in East and South Asia

M. Zhong et al.

Title Page
Abstract | Introduction
Conclusions | References
Tables | Figures
◀| |▶
◀ ▶
Back | Close
Full Screen / Esc
Printer-friendly Version
Interactive Discussion